

Article

A Novel Eco-Friendly Circular Approach to Comprehensive Utilizing Bittern Waste and Oyster Shell

Wei Pan ¹, Yucheng Yang ^{1,2,*} , Daomao Yang ¹, Moses Arowo ³, Shuai Wu ¹, Yingjie He ¹ and Qingyou Zeng ^{1,*}¹ College of Chemical Engineering, Huaqiao University, Xiamen 361021, China² Department of Chemical Engineering and Chemistry, Eindhoven University of Technology, 5600 MB Eindhoven, The Netherlands³ Department of Chemical & Process Engineering, Moi University, Eldoret 3900, Kenya

* Correspondence: yangyc@hqu.edu.cn (Y.Y.); tonyzeng@hqu.edu.cn (Q.Z.)

Abstract: Efficient waste management, especially in relation to swaste reuse, has become a pressing societal issue. The waste bittern generated during salt production and discarded oyster shells present formidable environmental challenges and a waste of resources for some coastal regions. Therefore, this work developed a two-stage circular process for the environmentally friendly and efficient utilization of both waste materials. In the first stage, CO₂ gas and an organic extraction phase comprising Tri(octyl-decyl)amine (R₃N) and isoamyl alcohol were introduced into the waste bittern to obtain MgCO₃·3H₂O (s). The second stage involved reacting the reacted organic extraction phase with oyster shell powders to produce CaCl₂·2H₂O (s) and CO₂ (g) and regenerate R₃N. This work focused on investigating the yield of MgCO₃·3H₂O and the regeneration ratio of R₃N, which are crucial indicators for the two stages involved in the process. The results indicate that, under optimal operating conditions, a maximum yield of 87% for MgCO₃·3H₂O was achieved, and the regeneration ratio of R₃N reached 97%. Furthermore, the reaction mechanism and thermodynamic functions of the R₃N regeneration process were elucidated as a crucial element in achieving a circular process. The findings of this work offer a sustainable solution to environmental pollution from waste bittern and oyster shells, and provide a promising avenue for green chemical production.

Keywords: waste reuse; recycling process; waste bittern; oyster shell; organic extraction



Citation: Pan, W.; Yang, Y.; Yang, D.; Arowo, M.; Wu, S.; He, Y.; Zeng, Q. A Novel Eco-Friendly Circular Approach to Comprehensive Utilizing Bittern Waste and Oyster Shell. *Processes* **2023**, *11*, 1209. <https://doi.org/10.3390/pr11041209>

Received: 21 March 2023

Revised: 7 April 2023

Accepted: 12 April 2023

Published: 14 April 2023



Copyright: © 2023 by the authors. Licensee MDPI, Basel, Switzerland. This article is an open access article distributed under the terms and conditions of the Creative Commons Attribution (CC BY) license (<https://creativecommons.org/licenses/by/4.0/>).

1. Introduction

Effective waste treatment and utilization, particularly of biomass wastes [1,2] and difficult-to-handle garbage [3], can promote sustainability and cost-effectiveness within green chemistry and engineering [4]. Waste bittern is a by-product of the salt-making industry and desalination processes, consisting mainly of solar bittern and sea bittern. Its release into the environment can have detrimental effects on living organisms [5,6]. Usually, the concentrations of magnesium ions and chloride ions in waste bittern are higher than those of other ions. Thus, the recovery of both salts can alleviate or eliminate environmental pollution associated with them.

There are several techniques for salt recovery. For instance, chloride ions are recycled by concentration, crystallization, and electrolysis [7–9], whereas magnesium ions are recycled by trioctylamine and N235 extraction [10,11], membrane electrolysis [9], and via the preparation of Mg(OH)₂, MgCO₃, and struvite [12–14]. However, these techniques for removing ions from waste bittern suffer from drawbacks such as secondary pollution, high costs, and low efficiency. Therefore, there is a need for an environmentally friendly and efficient process to treat waste bittern before disposal into the environment.

Oyster breeding is a thriving global industry that generates a significant by-product: oyster shells, consisting mainly of calcium carbonate (approximately 95%). However, these shells are frequently disposed of in coastal waters or landfills, resulting in the emission

of harmful gases, including NH_3 , H_2S , and amines, as well as water pollution and the proliferation of insect breeding sites exacerbating environmental pollution [15]. Many research studies suggest that oyster shells can be utilized in various ways, including as fillers in the material industry. Many research studies suggest diverse uses for oyster shells, including as fillers in the material industry [16,17], building material [18,19], composite material [20–22], and in chemical engineering for wastewater treatment [23,24], carbon dioxide absorption [25,26], catalysis [27,28], and as a source of calcium.

However, these alternative uses often involve processing single, cheap oyster shells with large amounts of chemical raw materials or energy, resulting in high costs and poor returns. To address these challenges, a new process should be developed that allows oyster shells and other waste materials to interact with each other. This reduces the need for additional chemicals or energy, ultimately leading to reduced costs and promoting the simultaneous reuse of multiple waste streams. This process represents a critical step toward the efficient and sustainable utilization of oyster shells and other waste materials.

Therefore, the work explores a novel environmentally friendly process that utilizes oyster shells and waste bittern, both of which are sourced from the sea, to produce magnesium carbonate and other by-products. Two stages are planned in this process. In the first stage, an organic extraction phase comprising R_3N , isoamyl alcohol, and CO_2 from oyster shells are introduced into a waste bittern to yield $\text{MgCO}_3 \cdot 3\text{H}_2\text{O}$. In the second stage, the used organic extraction phase is reacted with oyster shell powders to form $\text{CaCl}_2 \cdot 2\text{H}_2\text{O}$, CO_2 , and R_3N . Both R_3N and CO_2 are considered as recyclable materials and are reintroduced into the first stage. The process is optimized by systematically investigating the effects of reactant dosages, reaction time, stirring speed, temperature, and so on. Additionally, the reaction mechanism of the R_3N regeneration process, which is crucial to this process, was studied. Compared to previous relevant research, this process represents a significant advancement in the simultaneous and environmentally friendly utilization of two primary sea wastes to produce chemical products without generating any new waste. All by-products are recycled within the system, resulting in an efficient and sustainable process that effectively utilizes waste materials. Therefore, the results of this study provide a new perspective on the utilization of oyster shells and bittern.

2. Materials and Method

2.1. Materials

Waste bittern was obtained from Quanzhou Seawater Salt Factory in Quanzhou, China, and the oyster shells were sourced from a seafood market in Xiamen, China. They were characterized by an X-ray fluorescence spectrometer (ARL Perform'X 4200, Thermo Fisher Scientific, Waltham, MA, USA), and the results are shown in Tables 1 and 2, respectively. Ethylenediaminetetraacetic acid disodium salt dihydrate (EDTA, $\geq 99.5\%$, CAS: 60-00-4), zinc oxide ($\geq 99.0\%$, CAS: 1314-13-2), ammonia solution (25–28%, CAS: 1336-21-6), ammonium chloride ($\geq 99.5\%$, CAS: 12125-02-9), chrome black T (IND, CAS:1787-61-7), phenolphthalein (IND, CAS: 77-09-8), sodium hydroxide ($\geq 96.0\%$, CAS: 1310-73-2), calcium chloride ($\geq 96.0\%$, CAS: 10043-52-4), and isoamyl alcohol ($\geq 98.5\%$, CAS: 123-51-3) were all obtained as analytical reagents from Xilong Science Co., Ltd. (Guangdong, China). Hydrochloric acid (36.0–38.0%, CAS: 7647-01-0) and calcium-carboxylic acid indicator (IND, CAS: 3737-95-9) were supplied as analytical reagent by Sinopharm Chemical Reagent Co., Ltd. (Shanghai, China). Tri (octyl-decyl) amine (R_3N , $\geq 95\%$, 68814-95-9) was sourced as analytical reagent from Wuhan yuancheng co-create technology Co. Ltd. (Hubei, China). Carbon dioxide ($\geq 99.99\%$, CAS: 124-38-9) gas was from Quanzhou tianxing gas co. Ltd. (Fujian, China).

Table 1. Chemical composition of waste bittern.

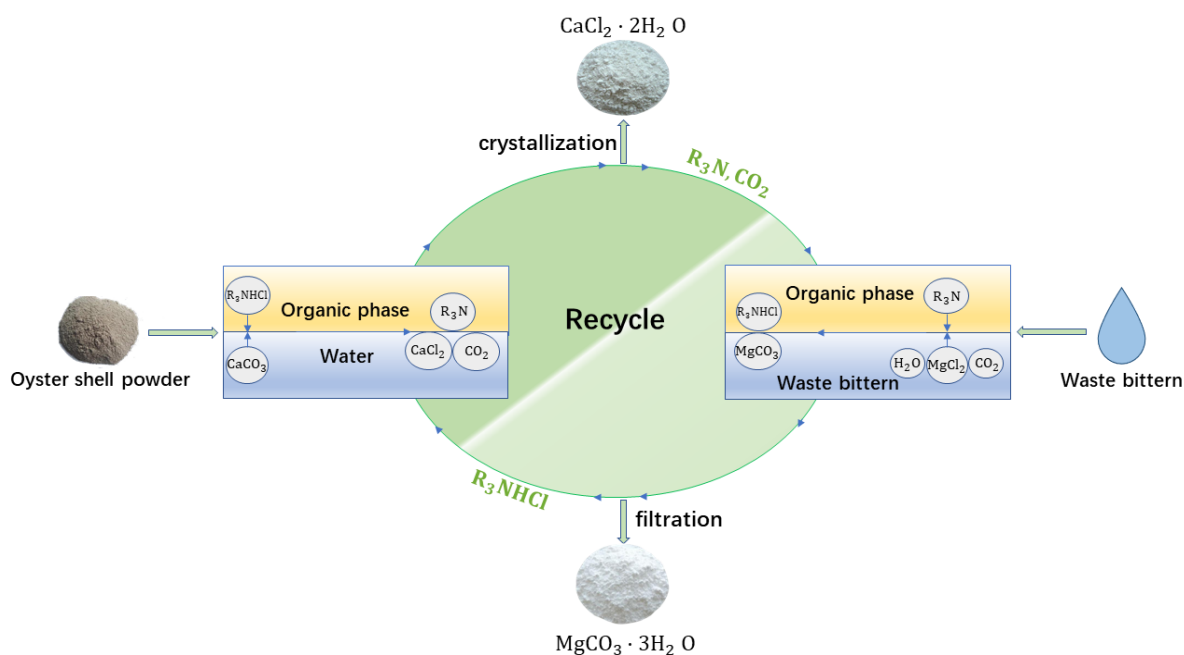
Element	Cl	Mg	Na	S	K	Al	Br
Mass fraction/%	18.24	4.76	4.15	2.71	1.35	0.54	0.25

Table 2. Chemical composition of oyster shell.

Element	Ca	Na	S	Cl	Mg	Si	Al
Mass fraction/%	21.29	0.64	0.20	0.42	0.21	0.09	0.05

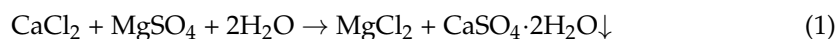
2.2. Method

The experimental process was divided into two parts, including waste bittern utilization process (Section 2.2.1) and oyster shell utilization process (Section 2.2.2). The process flow diagram is shown in Figure 1. All experiments were conducted thrice, and the maximum relative error observed was below 5%.

**Figure 1.** The process flow diagram of production of magnesium carbonate and calcium chloride from oyster shell and waste bittern.

2.2.1. Waste Bittern Utilization

The experimental process involved the mixing of waste bittern with CaCl_2 , resulting in the formation of $\text{CaSO}_4 \cdot 2\text{H}_2\text{O}$. The resultant mixture was subjected to a filtration process, which separated the solid $\text{CaSO}_4 \cdot 2\text{H}_2\text{O}$ residue from the waste bittern filtrate, which was free of SO_4^{2-} ions. The equation of the reaction is as follows:



The next step involved subjecting the waste bittern filtrate without SO_4^{2-} ions to a process that included mixing it with carbon dioxide, R_3N , and isoamyl alcohol using a half-moon impeller in a 1000 mL three-necked-flask at 313.15 K. Filtration of the resulting mixture yielded a solid residue of $\text{MgCO}_3 \cdot 3\text{H}_2\text{O}$ and a filtrate consisting of residual waste bittern and an organic solution [29–32]. The organic solution was subsequently employed in the oyster shell utilization process. The composition of the solid residue was analyzed using X-ray fluorescence spectroscopy (XRF), and the result is tabulated in Table 3. Based on these results, the maximum purity that can be achieved is 98.75% in this work.

Table 3. Chemical composition (%) of $\text{MgCO}_3 \cdot 3\text{H}_2\text{O}$ as analyzed by XRF.

Compound	Mg	Ca	Si	S	Al
Wt%	50.13	0.996	0.059	0.035	0.042

The equation of the reaction in this step is as follows:



The effects of different operating parameters, including the dosages of waste bittern, R_3N , and isoamyl alcohol, reaction time, and stirring speed, on the yield of $\text{MgCO}_3 \cdot 3\text{H}_2\text{O}$ was systematically investigated. Further details on the characterization of the relevant substances in the waste bittern utilization process can be found in Appendix A. The yield of $\text{MgCO}_3 \cdot 3\text{H}_2\text{O}$ was calculated as follows:

$$\lambda_1 = \frac{n_1}{n} \times 100\% \quad (3)$$

where λ_1 denotes the yield of $\text{MgCO}_3 \cdot 3\text{H}_2\text{O}$, n_1 represents the moles of $\text{MgCO}_3 \cdot 3\text{H}_2\text{O}$, and n represents the moles of magnesium in the waste bittern. The number of moles was determined by measuring the concentration of magnesium ion through titration method and calculating the volume used.

The titration method involved two steps. In the first step, the sample was diluted 100 times and mixed with triethanolamine solution, potassium hydroxide solution, and calcium–carboxylic acid indicator to determine the concentration of calcium ion. The resulting solution was titrated with a known concentration of EDTA solution (0.0213 M) until the color changed from purple to blue. In the second step, another sample from same solution was also diluted 100 times and mixed with triethanolamine solution, potassium hydroxide solution, ammonia–ammonium chloride solution, and chrome black T solution to determine the concentration of magnesium ion. This mixture was titrated with the known concentration of EDTA solution (0.0213 M) until the color changed from purple to blue. The concentration of magnesium ions was calculated based on the volume of twice-EDTA-used solution. Each titration experiment was repeated three times, and the relevant titration data can be found in Appendix B.

2.2.2. Oyster Shell Utilization

Initially, the oyster shells were thoroughly washed and ground into a fine powder. Next, the purified oil phase obtained from the first stage process, which contained $\text{R}_3\text{N} \cdot \text{HCl}$, was blended with the oyster shell powder and distilled water to produce R_3N , CaCl_2 , and CO_2 . Calcium chloride dihydrate was then acquired by crystallizing a calcium chloride solution. The composition of $\text{CaCl}_2 \cdot 2\text{H}_2\text{O}$ was evaluated using XRF, and the corresponding results are provided in Table 4. Based on these results, the maximum that can be achieved is 96.63%.

Table 4. Chemical composition (%) of $\text{CaCl}_2 \cdot 2\text{H}_2\text{O}$ as analyzed by XRF.

Compound	Cl	Ca	Mg	Na	S
Wt%	52.79	31.38	0.694	0.622	0.217

The chemical reaction is as follows:



The characterizations of the relevant substances involved in the oyster shell utilization process can be found in Appendix A.

Although obtaining $\text{CaCl}_2 \cdot 2\text{H}_2\text{O}$ is an essential objective in the oyster shell utilization process, the regeneration of R_3N is even more crucial because it plays a pivotal role in achieving a continued cycle in the two-stage process. Specifically, the occurrence of the R_3N regeneration reaction directly impacts the feasibility of the circle process, while also positively affecting the conversion rate of calcium chloride. Therefore, the regeneration

ratio of R_3N is a crucial assessment index for this process, and it was determined using the following calculation:

$$\lambda_2 = \frac{n_0(R_3N \cdot HCl) - n_r(R_3N \cdot HCl)}{n_0(R_3N \cdot HCl)} \times 100\% \quad (5)$$

where λ_2 represents the regeneration ratio of the R_3N , and $n_r(R_3N \cdot HCl)$ and $n_0(R_3N \cdot HCl)$ denote the final and initial moles of $R_3N \cdot HCl$ in process, respectively. The molar concentration of $R_3N \cdot HCl$ was determined through titration using a calibrated NaOH solution. The effects of operating parameters, including phase ratio between aqueous and oil phases and reaction temperature, on the regeneration ratio were investigated. Additionally, the thermodynamic function and reaction mechanism of the regeneration process were established in this work.

3. Results and Discussion

3.1. Effects of the Operating Conditions

3.1.1. Effect of Phase Ratio of Reactants on the Yield of $MgCO_3 \cdot 3H_2O$

Figure 2 presents the effects of the phase ratio of waste bittern, R_3N , and isoamyl alcohol on the yield of $MgCO_3 \cdot 3H_2O$. Figure 2a shows an increase in the phase ratio between R_3N and waste bittern, and an initial improvement in the yield of $MgCO_3 \cdot 3H_2O$ followed by a subsequent decrease. The results demonstrate that R_3N , as an extractant, directly impacts the yield of the process. However, due to the high viscosity of R_3N , the mixing efficiency between reactants is reduced when the phase ratio between R_3N and waste bittern is larger than 4.8, ultimately resulting in a decrease in the yield. Isoamyl alcohol, as a diluent, has the capability of reducing the viscosity of the organic solution. Therefore, Figure 2b demonstrates that the addition of isoamyl alcohol improves the yield of $MgCO_3 \cdot 3H_2O$ by increasing the probability of contact between reactants through the viscosity reduction. However, when the dosage of isoamyl alcohol is higher, it can surround R_3N molecules, thereby hindering the contact between reactants and R_3H and ultimately resulting in a decrease in the yield. The results show that the best improvement in the yield of $MgCO_3 \cdot 3H_2O$ is achieved when the phase ratio of isoamyl alcohol is the same as that of R_3H . The optimal phase ratio of waste bittern, R_3N , and isoamyl alcohol in this work for achieving the highest yield is 1:4.8:4.8, respectively, which results in a yield of 87%.

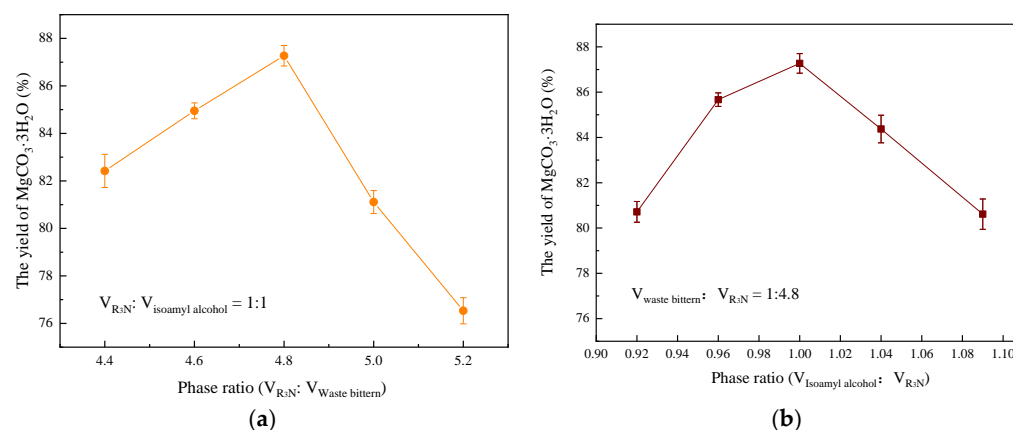


Figure 2. Effect of phase ratio of reactants on the yield of $MgCO_3 \cdot 3H_2O$ at reaction time = 7 h, stirring speed = 600 rpm, and reaction temperature = 313.15 K: (a) the phase ratio between R_3N and water bittern; (b) the phase ratio between isoamyl alcohol and R_3N .

3.1.2. Effect of Reaction Time and Stirring Speed on the Yield of $MgCO_3 \cdot 3H_2O$

The effects of the reaction time and stirring speed on the yield of $MgCO_3 \cdot 3H_2O$ are shown in Figure 3. As seen in Figure 3a, the yield of $MgCO_3 \cdot 3H_2O$ increased with an increasing reaction time and balanced at the 7th hour, after which there was no significant

change in the yield, indicating that the reaction had reached its optimal point. Longer reaction times resulted in more extraction reactions between the reactant molecules and a higher yield of $\text{MgCO}_3 \cdot 3\text{H}_2\text{O}$; further increases in time had a limited effect on the yield. Therefore, an optimal reaction time of 7 h can be used to obtain a high yield of $\text{MgCO}_3 \cdot 3\text{H}_2\text{O}$ in this work.

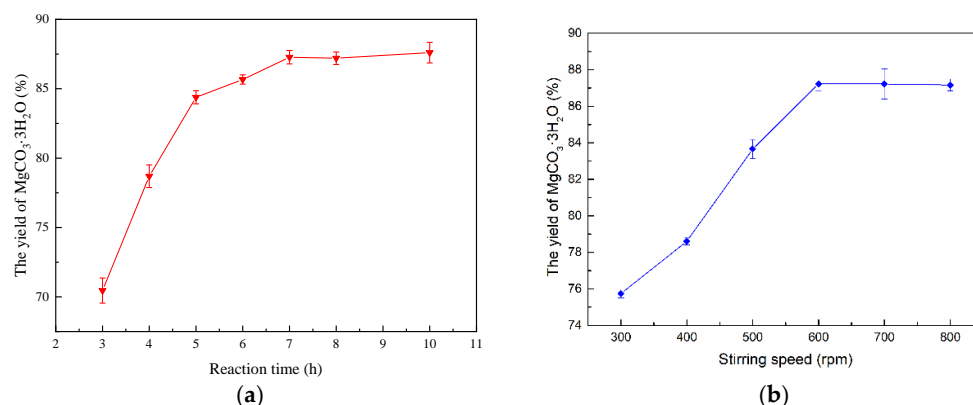


Figure 3. Effect of (a) reaction time (stirring speed = 600 rpm) and (b) stirring speed (reaction time = 7 h) on the yield of $\text{MgCO}_3 \cdot 3\text{H}_2\text{O}$ at $V_{\text{waste bitters}}: V_{\text{R3N}}: V_{\text{isoamyl alcohol}} = 1:4.8:4.8$ and reaction temperature = 313.15 K.

It is evident from Figure 3b that the yield of $\text{MgCO}_3 \cdot 3\text{H}_2\text{O}$ gradually increased with an increase in stirring speed from 300 to 600 rpm and then remained generally constant. This is due to the fact that, at low stirring speeds, the oil phase and water phase were not mutually soluble, making it difficult for the reactants to come into adequate contact. A higher stirring speed, on the other hand, increased the contact between the reactants, resulting in an increased reaction rate and a higher yield of $\text{MgCO}_3 \cdot 3\text{H}_2\text{O}$. However, there is a limit to the mixing capacity with a further increase in stirring, and higher stirring speeds also mean a higher energy consumption. Therefore, the optimal stirring speed can be established as 600 rpm in this work.

3.1.3. Effect of Phase Ratio of the Aqueous and Oil Phase on R_3N Regeneration Rate

The regeneration rate of R_3N increased gradually up to a maximum of 97% as the phase ratio of aqueous and oil phases rose from 0.0 to 0.67 and then remained relatively constant, as shown in Figure 4. Hydrochloric acid was produced during the regeneration process of R_3H chemically with oyster shell powder, thereby improving the regeneration rate. Without the aqueous phase, it is difficult for the hydrochloric acid in oil phase to directly react with oyster shell powder, and the regeneration rate will be greatly reduced. However, the presence of an aqueous phase can dissolve hydrochloric acid from the oil phase and a small amount of oyster shell powder and quickly initiate a chemical reaction between the two substances, thereby promoting an increase in the regeneration rate of R_3N . Therefore, increasing the phase ratio between the aqueous and oil solutions up to 0.67 is beneficial for improving the regeneration rate. However, when the phase ratio is further increased, the molecular exchange between the oil and aqueous phases may be nearing saturation, leading to the regeneration rate of $\text{R}_3\text{N} \cdot \text{HCl}$ no longer growing, or even decreasing, due to a reduction in the concentration of hydrochloric acid in the aqueous solution that reduces the mass transfer between the two phases. According to Figure 4, the optimal phase ratio of the aqueous and oil phase can be set as 0.67 in this work.

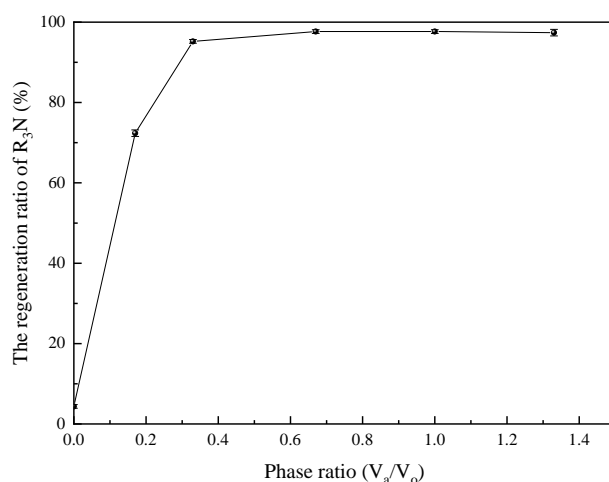


Figure 4. Effect of phase ratio between aqueous and oil phases on R_3N regeneration rate at stirring speed = 300 rpm, reaction time = 420 s, and reaction temperature = 353.15 K.

3.1.4. Effect of Reaction Temperature on R_3N Regeneration Rate

According to the data presented in Figure 5, the regeneration rate of R_3N increased with an increase in the reaction temperature up to 318.15 K, achieving a maximum of 97%. Subsequently, the regeneration rate remained almost constant with a further rise in temperature. The R_3N regeneration process is known to be endothermic, and detailed information can be found in Section 3.2. The higher reaction temperature facilitated the decomposition rate of $R_3N \cdot HCl$, resulting in an increased yield of R_3N . However, temperatures beyond 358.15 K could cause the solvent in the oil phase to evaporate rapidly, leading to an increase in concentration and a slight reduction in the regeneration rate of R_3N .

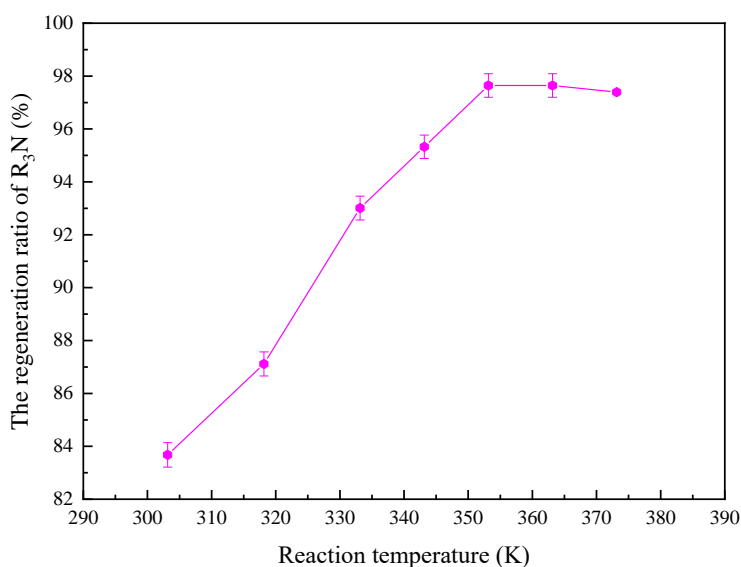


Figure 5. Effect of reaction temperature on regeneration rate of R_3N at stirring speed = 300 rpm, reaction time = 420 s, and $V_a:V_o = 0.67$.

3.2. Thermodynamic Function Calculation and Reaction Mechanism of the R_3N Regeneration Process

The reaction mechanism of the R_3N regeneration process was investigated in this work. The organic regeneration solution of R_3N , an aqueous solution of $CaCl_2$, and CO_2 gas were obtained by heating a mixture of the oil phase ($R_3N \cdot HCl$), distilled water, and

oyster shell powder. The reaction equation is expressed as Equation (4). According to the equation, the equilibrium constant calculation expression is as follows:

$$K = \frac{[CaCl_{2(w)}][R_3N_{(o)}]^2}{[R_3N \cdot HCl_{(o)}]^2} \quad (6)$$

The equilibrium constants at different temperatures were calculated, and the results are listed in Table 5.

Table 5. Equilibrium concentrations and equilibrium constants at different temperatures.

T/(K)	$c(R_3N \cdot H^+)_{(o)}/(mol/L)$	$c(CaCl_2)_{(w)}/(mol/L)$	$c(R_3N)_{(o)}/(mol/L)$	ln K
353.15	0.032	0.603	2.065	7.798
343.15	0.046	0.594	2.052	7.081
333.15	0.066	0.579	2.034	6.313
323.15	0.086	0.564	2.012	5.736
318.15	0.106	0.549	1.992	5.270
302.15	0.139	0.524	1.959	4.642

According to van't Hoff equation,

$$\ln K = -\frac{\Delta H}{RT} + C \quad (7)$$

where K is the equilibrium constant, ΔH denotes the enthalpy change ($J \cdot mol^{-1}$), R is the molar gas constant ($R = 8.314 J \cdot mol^{-1} \cdot K^{-1}$), T is the absolute temperature (K), and C is a constant. Figure 6 displays the linear relationship between $\ln K$ and $1/T$. The reaction was found to be endothermic, as evidenced by the negative slope of the line. The value of the slope was used to calculate ΔH , which was determined to be $56.0 kJ \cdot mol^{-1}$.

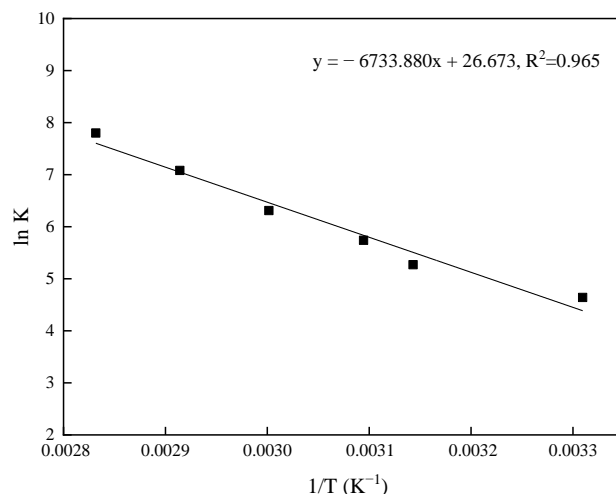


Figure 6. The linear relationship between $\ln K$ and $1/T$.

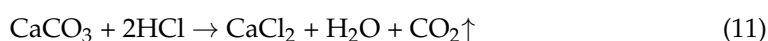
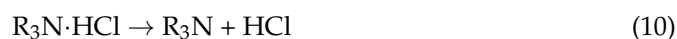
The Gibbs function change (ΔG) and the entropy change (ΔS) of reaction (4) were calculated using the equilibrium constant and Gibbs function as follows:

$$\Delta G = \Delta H - T\Delta S \quad (8)$$

$$\Delta G = -RT \ln K \quad (9)$$

The values obtained at 298.15 K were $-10.1 \text{ kJ}\cdot\text{mol}^{-1}$ and $221.8 \text{ J}\cdot\text{mol}^{-1}\cdot\text{K}$, respectively, indicating that the reaction can occur spontaneously at room temperature despite being endothermic. However, a higher temperature favors the yield of CaCl_2 , the overall reaction progress, and the regeneration rate of R_3N .

Reaction (4) can be divided into two steps, expressed as Equation (10) and Equation (11), respectively:



The standard thermodynamic data of Reaction (11) is shown in Table 6, and the thermodynamic functions of reaction (11) are calculated as $\Delta H = -83.2 \text{ kJ}\cdot\text{mol}^{-1}$, $\Delta G = -60.9 \text{ kJ}\cdot\text{mol}^{-1}$ and $\Delta S = -76.7 \text{ J}\cdot\text{mol}^{-1}\cdot\text{K}^{-1}$ at 298.15 K. The results indicate that reaction (11) is exothermic and can occur spontaneously under room temperature and atmospheric pressure, without the need for additional energy.

Table 6. Thermodynamic functions data of reaction (11).

Thermodynamic Functions (298.15 K)	CaCO_3	HCl	CaCl_2	H_2O	CO_2
$\Delta_f H_m$ (KJ/mol)	-1206.92	-92.307	-795.4	-285.83	-393.509
$\Delta_f G_m$ (KJ/mol)	-1128.79	-95.299	-748.8	-237.129	-394.359
S_m (J/mol/K)	92.9	186.908	108.4	69.91	213.74

According to the calculation rules governing thermodynamic functions of related reactions, reaction (10) has thermodynamic values of $\Delta H = 69.6 \text{ kJ}\cdot\text{mol}^{-1}$, $\Delta G = 25.4 \text{ kJ}\cdot\text{mol}^{-1}$, and $\Delta S = 149.2 \text{ J}\cdot\text{mol}^{-1}\cdot\text{K}^{-1}$ at 298.1 K. These values indicate that the decomposition process of $\text{R}_3\text{N}\cdot\text{HCl}$ is endothermic and cannot occur spontaneously at room temperature.

The combination of reactions (10) and (11), achieved by adding oyster shell powder to the $\text{R}_3\text{N}\cdot\text{HCl}$ solution, reduces the activation energy of the entire reaction, facilitating the decomposition of $\text{R}_3\text{N}\cdot\text{HCl}$ at low temperatures and enabling a high conversion with minimal heat input. This approach is environmentally friendly and practical, not requiring harsh reaction conditions. The results also demonstrate the superiority and feasibility of the joint utilization of oyster shells and waste bittern.

4. Conclusions

This work developed an innovative, environmentally friendly two-stage process that utilizes oyster shells and waste bittern to produce magnesium carbonate and calcium chloride. In the first stage, a mixture of CO_2 , R_3N , and isoamyl alcohol is injected into a waste bittern to obtain $\text{MgCO}_3\cdot 3\text{H}_2\text{O}$. The organic extraction phase from the first stage then reacts with the oyster shell to produce $\text{CaCl}_2\cdot 2\text{H}_2\text{O}$, CO_2 , and R_3N in the second stage. The optimal conditions for the process were established as follows: in the first stage, a maximum yield of 87% for $\text{MgCO}_3\cdot 3\text{H}_2\text{O}$ was obtained, with a phase ratio of waste bittern, R_3N , and isoamyl alcohol of 1:4.8:4.8, a reaction time of 7 h, and a stirring speed of 600 rpm. In the second stage, the regeneration rate of R_3N reached a maximum of 97% at a reaction temperature of 358.15 K and a phase ratio of 0.67 between the aqueous and oil phases. The process generates nearly zero waste as all by-products are recycled in the system, solving the problem of environmental pollution caused by waste bittern and oyster shells. This technology provides a new perspective for green chemical production. For future industrial applications, two main challenges in this system should be addressed: (1) the development of a more effective design for multiphase reactors to improve the efficiency of mixing and finally enhance the reaction and regeneration ratios, and (2) the optimization of the circulation efficiency of R_3N , which is a crucial component that connects two stages, to reduce its loss and ensure its efficacy for future applications.

Author Contributions: Conceptualization: Q.Z. and W.P.; methodology: W.P. and S.W.; validation: D.Y. and Y.H.; formal analysis: W.P. and D.Y.; investigation: W.P.; resources: Q.Z.; data curation: W.P. and Y.Y.; writing—original draft preparation: W.P.; writing—review and editing: Y.Y. and M.A.; visualization: Y.Y.; supervision: Y.Y. and Q.Z. All authors have read and agreed to the published version of the manuscript.

Funding: This research was funded by Industry-university-research collaboration project of Xiamen grant number [2022CXY02010].

Data Availability Statement: The data used to support the findings of this study are available from the corresponding author upon request.

Acknowledgments: The Instrumental Analysis Centre of Huaqiao University for analytical characterization is acknowledged.

Conflicts of Interest: The authors declare no conflict of interest.

Appendix A

Appendix A.1. Characterization Methods

The characteristic functional groups present in the oil phase were analyzed by Fourier transform infrared spectroscopy (FT-IR) over a range of 1000–3000 cm^{-1} . The structural analysis and identification of $\text{MgCO}_3 \cdot 3\text{H}_2\text{O}$, $\text{CaSO}_4 \cdot 2\text{H}_2\text{O}$, and $\text{CaCl}_2 \cdot 2\text{H}_2\text{O}$ were conducted by powder X-ray diffraction (XRD), employing Cu $K\alpha$ radiation ($\lambda = 1.5406 \text{ \AA}$) within a range of 2θ from 5° to 80° . The analysis results were generated using Jade software 5.0.

Appendix A.2. Characterization Results

Appendix A.2.1. The Fourier Transform Infrared Spectroscopy

The occurrence of the extraction reaction was confirmed using Fourier transform infrared spectroscopy, and the results are presented in Figure A1.

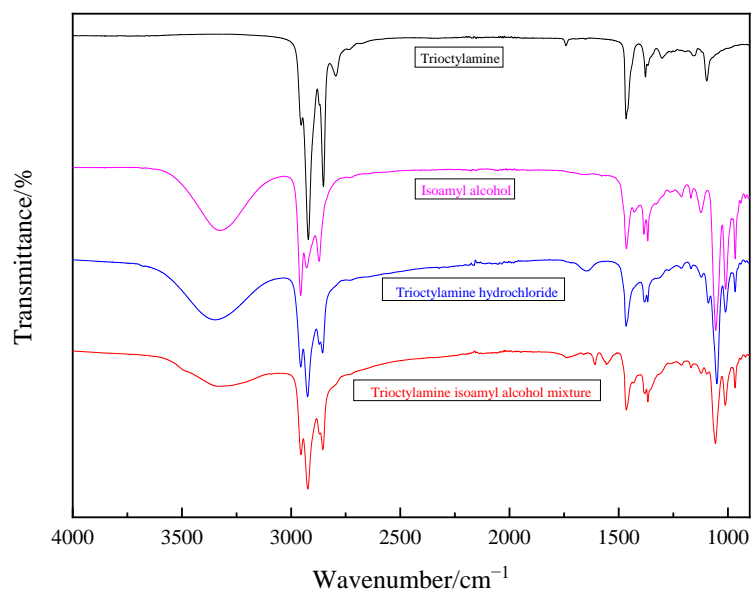


Figure A1. FT-IR spectra of R_3N , isoamyl alcohol, $\text{R}_3\text{N} \cdot \text{HCl}$, and the mixture of R_3N and isoamyl alcohol.

The stretching bands of the O–H vibration were observed within the range of 3347–3327 cm^{-1} . When the extraction reaction did not occur, two types of hydrogen bonds, namely $\text{R}_3\text{N} \cdots \text{O}-\text{H}$ and $\text{H}-\text{O} \cdots \text{H}-\text{O}$, were identified. Upon comparing the three stretching vibration bands within the 3347–3327 cm^{-1} range, the peak of $\text{R}_3\text{N} \cdot \text{HCl}$ was observed to shift 20 cm^{-1} higher, indicating the transformation of the hydrogen bonds from

$R_3N\cdots O-H$ and $H-O\cdots H-O$ to $R_3NH+\cdots O-H$ and the occurrence of the extraction reaction. The stretching bands of the N–H vibration were observed in the range of $2700\text{--}2500\text{ cm}^{-1}$, and the presence of $R_3NH+\cdots O-H$ in $R_3N\cdot HCl$ led to a greater intensity and breadth of the N–H peak compared to other spectra. The stretching bands of the C–N vibration were observed at 1096 cm^{-1} . Upon transformation from $R_3N\cdots O-H$ to $R_3NH+\cdots O-H$, the peaks of the C–N stretching vibration shifted from 1096 to 1050 cm^{-1} [33].

Appendix A.2.2. The X-ray Diffraction Spectra for Products ($MgCO_3\cdot 3H_2O$ and $CaCl_2\cdot 2H_2O$)

The diffraction patterns obtained from X-ray powder diffraction (XRD) analysis, as shown in Figure A2, exhibit a precise match with the diffraction patterns of $MgCO_3\cdot 3H_2O$ and $CaCl_2\cdot 2H_2O$ in the PDF-70-1433 and PDF-70-0385 databases, respectively. This result confirms that the products obtained from the process are indeed $MgCO_3\cdot 3H_2O$ and $CaCl_2\cdot 2H_2O$. Additionally, the narrow peaks observed in the XRD patterns indicate the high crystallinity of the products, and the absence of any impurity peaks confirms the high purity of the products.

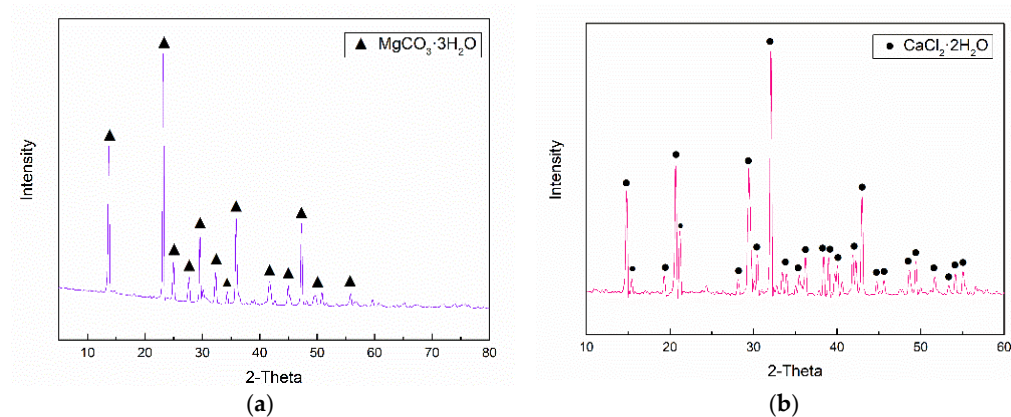


Figure A2. XRD patterns of (a) $MgCO_3\cdot 3H_2O$ and (b) $CaCl_2\cdot 2H_2O$.

Appendix B

The calcium ions and magnesium ions concentration were calculated according to Equations (A1) and (A2):

$$C_1 = \frac{\frac{V_1}{1000} \times cM_1 \times 1000}{\frac{V}{1000}} \quad (A1)$$

$$C_2 = \frac{\frac{V_2}{1000} - \frac{V_1}{1000} \times cM_2 \times 1000}{\frac{V}{1000}} \quad (A2)$$

where C_1 represents the mass concentration of calcium ions (mg/L), C_2 represents the mass concentration of magnesium ions (mg/L), V_1 represents the volume of the EDTA solution used for titrating calcium ions (mL), V_2 represents the volume of the EDTA solution used for titrating magnesium ions (mL), c represents the molar concentration of EDTA (mol/L), M_1 represents the molar mass of calcium (g/mol) ($M_1 = 40.08$), M_2 represents the molar mass of magnesium (g/mol) ($M_2 = 24.31$), and V represents the volume of the water in which the waste bittern was diluted.

For example, the results for a sample are shown in Table A1.

Table A1. The results of magnesium ions concentration in a sample.

Sequence of Experiments	Water Sample Volume/mL	EDTA Volume /mL	Magnesium Ions' Concentration/g/L
1	50.00	54.55	56.49
2	50.00	55.20	57.17
3	50.00	55.15	57.11
Average value	50.00	54.97	56.92

References

- Alammar, A.; Hardian, R.; Szekely, G. Upcycling agricultural waste into membranes: From date seed biomass to oil and solvent-resistant nanofiltration. *Green Chem.* **2022**, *24*, 365–374. [[CrossRef](#)]
- Kita, Y.; Amao, Y. Visible-light-driven 3-hydroxybutyrate production from acetone and low concentrations of CO₂ with a system of hybridized photocatalytic NADH regeneration and multi-biocatalysts. *Green Chem.* **2023**, *25*, 2699–2710. [[CrossRef](#)]
- Cavalcante, J.; Hardian, R.; Szekely, G. Antipathogenic upcycling of face mask waste into separation materials using green solvents. *SM&T* **2022**, *32*, e00448. [[CrossRef](#)]
- Zhang, N.; Moment, A. Upcycling Construction and Demolition Waste into Calcium Carbonates: Characterization of Leaching Kinetics and Carbon Mineralization Conditions. *ACS Sustain. Chem. Eng.* **2023**, *11*, 866–879. [[CrossRef](#)]
- Mustafa, J.; Mourad, A.A.H.I.; Al-Marzouqi, A.H.; El-Naas, M.H. Simultaneous treatment of reject brine and capture of carbon dioxide: A comprehensive review. *Desalination* **2020**, *483*, 114386. [[CrossRef](#)]
- Panagopoulos, A.; Haralambous, K.J.; Loizidou, M. Desalination brine disposal methods and treatment technologies—A review. *Sci. Total. Environ.* **2019**, *693*, 133545. [[CrossRef](#)] [[PubMed](#)]
- Sun, J.; Dong, Y.; Kong, C. Manufacture of sodium-free lithium chloride from salt lake brine. *Sep. Purif. Technol.* **2014**, *136*, 309–313. [[CrossRef](#)]
- Guo, X.F.; Li, D.; Liu, J.L.; Wang, Z.R.; Wang, J.; Zhao, Y.Y.; Yuan, J.S. Separation of sodium and potassium using adsorption—Elution/crystallization scheme from bittern. *Chem. Eng. Res. Des.* **2020**, *161*, 72–81. [[CrossRef](#)]
- Pan, X.J.; Dou, Z.H.; Zhang, T.A.; Meng, D.L.; Fan, Y.Y. Separation of metal ions and resource utilization of magnesium from saline lake brine by membrane electrolysis. *Sep. Purif. Technol.* **2020**, *251*, 117316. [[CrossRef](#)]
- Yu, X.; Cui, J.; Liu, C.; Yuan, F.; Guo, Y.; Deng, T. Separation of magnesium from high Mg/Li ratio brine by extraction with an organic system containing ionic liquid. *Chem. Eng. Sci.* **2020**, *229*, 116019. [[CrossRef](#)]
- Viirolainen, S.; Fallah Fini, M.; Miettinen, V.; Laitinen, A.; Haapalainen, M.; Sainio, T. Removal of calcium and magnesium from lithium brine concentrate via continuous counter-current solvent extraction. *Hydrometallurgy* **2016**, *162*, 9–15. [[CrossRef](#)]
- Mohammad, A.F.; El-Naas, M.H.; Al-Marzouqi, A.H.; Suleiman, M.I.; Al Musharfy, M. Optimization of magnesium recovery from reject brine for reuse in desalination post-treatment. *J. Water Process. Eng.* **2019**, *31*, 100810. [[CrossRef](#)]
- Bang, J.H.; Chae, S.C.; Lee, S.W.; Kim, J.W.; Song, K.; Kim, J.; Kim, W. Sequential carbonate mineralization of desalination brine for CO₂ emission reduction. *J. CO₂ Util.* **2019**, *33*, 427–433. [[CrossRef](#)]
- Wang, J.; Ye, X.; Zhang, Z.; Ye, Z.L.; Chen, S. Selection of cost-effective magnesium sources for fluidized struvite crystallization. *J. Environ. Sci.* **2018**, *70*, 144–153. [[CrossRef](#)]
- Freitas de Alvarenga, R.A.; Galindro, B.M.; Helpa, C.F.; Soares, S.R. The recycling of oyster shells: An environmental analysis using life cycle assessment. *J. Environ. Manag.* **2012**, *106*, 102–109. [[CrossRef](#)]
- Hamester, M.R.R.; Balzer, P.S.; Becker, D. Characterization of calcium carbonate obtained from oyster and mussel shells and incorporation in polypropylene. *Mater. Res.* **2012**, *15*, 204–208. [[CrossRef](#)]
- Tongamp, W.; Kano, J.; Zhang, Q.; Saito, F. Simultaneous treatment of PVC and oyster-shell wastes by mechanochemical means. *Waste Manag.* **2008**, *28*, 484–488. [[CrossRef](#)]
- Yoon, G.L.; Kim, B.T.; Kim, B.O.; Han, S.H. Chemical–mechanical characteristics of crushed oyster-shell. *Waste Manag.* **2003**, *23*, 825–834. [[CrossRef](#)]
- Lertwattanakul, P.; Makul, N.; Siripattaraprat, C. Utilization of ground waste seashells in cement mortars for masonry and plastering. *J. Environ. Manag.* **2012**, *111*, 133–141. [[CrossRef](#)]
- Lertcumfu, N.; Jaita, P.; Manotham, S.; Jarupoom, P.; Eitssayeam, S.; Pengpat, K.; Rujijjanagul, G. Properties of calcium phosphates ceramic composites derived from natural materials. *Ceram. Int.* **2016**, *42*, 10638–10644. [[CrossRef](#)]
- Chen, B.; Peng, X.; Wang, J.G.; Wu, X. Laminated microstructure of Bivalva shell and research of biomimetic ceramic/polymer composite. *Ceram. Int.* **2004**, *30*, 2011–2014. [[CrossRef](#)]
- Hoque, M.E. Processing and Characterization of Cockle Shell Calcium Carbonate (CaCO₃) Bioceramic for Potential Application in Bone Tissue Engineering. *J. Mater. Sci.* **2013**, *2*, 132. [[CrossRef](#)]
- Jung, S.; Heo, N.S.; Kim, E.J.; Oh, S.Y.; Lee, H.U.; Kim, I.T.; Hur, J.; Lee, G.W.; Lee, Y.C.; Huh, Y.S. Feasibility test of waste oyster shell powder for water treatment. *Process Saf. Environ.* **2016**, *102*, 129–139. [[CrossRef](#)]
- Kwon, H.B.; Lee, C.W.; Jun, B.S.; Yun, J.d.; Weon, S.Y.; Koopman, B. Recycling waste oyster shells for eutrophication control. *Resour. Conserv. Recycl.* **2004**, *41*, 75–82. [[CrossRef](#)]

25. Ma, K.W.; Teng, H. CaO Powders from Oyster Shells for Efficient CO₂ Capture in Multiple Carbonation Cycles. *J. Am. Ceram. Soc.* **2010**, *93*, 221–227. [[CrossRef](#)]
26. Li, Y.J.; Zhao, C.S.; Chen, H.C.; Duan, L.B.; Chen, X.P. CO₂ Capture Behavior of Shell during Calcination/Carbonation Cycles. *Chem. Eng. Technol.* **2009**, *32*, 1176–1182. [[CrossRef](#)]
27. Viriya-Empikul, N.; Krasae, P.; Puttasawat, B.; Yoosuk, B.; Chollacoop, N.; Faungnawakij, K. Waste shells of mollusk and egg as biodiesel production catalysts. *Bioresour. Technol.* **2010**, *101*, 3765–3767. [[CrossRef](#)] [[PubMed](#)]
28. Buasri, A.; Chaiyut, N.; Loryuenyong, V.; Worawanitchaphong, P.; Trongyong, S. Calcium oxide derived from waste shells of mussel, cockle, and scallop as the heterogeneous catalyst for biodiesel production. *Sci. World J.* **2013**, *2013*, 460923. [[CrossRef](#)]
29. Wang, W.; Wang, M.; Liu, X.; Wang, P.; Xi, Z. Experiment and Optimization for Simultaneous Carbonation of Ca(2+) and Mg(2+) in A Two-phase System of Insoluble Diisobutylamine and Aqueous Solution. *Sci. Rep.* **2015**, *5*, 10862. [[CrossRef](#)] [[PubMed](#)]
30. Liu, X.; Wang, W.; Wang, M.; Wang, P. Experimental Study of CO₂ Mineralization in Ca²⁺-Rich Aqueous Solutions Using Tributylamine as an Enhancing Medium. *Energy Fuels* **2014**, *28*, 2047–2053. [[CrossRef](#)]
31. Zhou, Z.; Liang, F.; Qin, W.; Fei, W. Coupled reaction and solvent extraction process to form Li₂CO₃: Mechanism and product characterization. *AIChE J.* **2014**, *60*, 282–288. [[CrossRef](#)]
32. Chen, G.; Song, X.; Dong, C.; Sun, S.; Sun, Z.; Yu, J. Mineralizing CO₂ as MgCO₃·3H₂O Using Abandoned MgCl₂ Based on a Coupled Reaction–Extraction–Alcohol Precipitation Process. *Energy Fuels* **2016**, *30*, 7551–7559. [[CrossRef](#)]
33. Li, Y.; Song, X.; Chen, G.; Sun, S.; Xu, Y.; Yu, J. Extraction of hydrogen chloride by a coupled reaction-solvent extraction process. *Front. Chem. Sci. Eng.* **2015**, *9*, 479–487. [[CrossRef](#)]

Disclaimer/Publisher’s Note: The statements, opinions and data contained in all publications are solely those of the individual author(s) and contributor(s) and not of MDPI and/or the editor(s). MDPI and/or the editor(s) disclaim responsibility for any injury to people or property resulting from any ideas, methods, instructions or products referred to in the content.